

# Measuring the mass profile of galaxy clusters beyond their virial radius

ANTONALDO DIAFERIO

*Dipartimento di Fisica Generale “Amedeo Avogadro”, Università degli Studi di Torino  
Via P. Giuria 1, I-10125 Torino, Italy*

*Istituto Nazionale di Fisica Nucleare, Sezione di Torino,  
Via P. Giuria 1, I-10125 Torino, Italy*

**Summary.** — Traditional estimators of the mass of galaxy clusters assume that the cluster components (galaxies, intracluster medium, and dark matter) are in dynamical equilibrium. Two additional estimators, that do not require this assumption, were proposed in the 1990s: gravitational lensing and the caustic technique. With these methods, we can measure the cluster mass within radii much larger than the virial radius. In the caustic technique, the mass measurement is only based on the celestial coordinates and redshifts of the galaxies in the cluster field of view; therefore, unlike lensing, it can be, in principle, applied to clusters at any redshift. Here, we review the origin, the basics and the performance of the caustic method.

## 1. – Introduction

In the currently accepted cosmological model, galaxy formation is intimately connected to the formation of the large-scale cosmic structure. To test this model, we need to measure the relative distribution of light and matter in the Universe. The mass distribution on small scales, from galaxies to galaxy clusters, has been usually inferred by

assuming that systems are in dynamical equilibrium. On very large scales, the mass overdensities are small enough that the linear theory of density perturbations can be used to measure the mass distribution from the relation between the mass density field and the peculiar velocities of galaxies [80].

On intermediate, mildly non-linear scales,  $\sim 1-10h^{-1}$  Mpc,<sup>(1)</sup> neither the dynamical equilibrium hypothesis nor linear theory are valid. No robust way of measuring the mass distribution in this regime was available until the 1990s, when both gravitational lensing and the caustic technique were developed. Here, we provide an overview of how the caustic technique came about and what it has contributed so far.

## 2. – The context of mass estimators

**2.1. The assumption of dynamical equilibrium.** – Galaxy cluster mass estimators measure either the total mass within a given radius  $R$  or the mass radial profile. Traditionally, both kinds of estimators are based on the assumption that the cluster is spherical and in dynamical equilibrium.

The virial theorem is usually applied when the number of galaxy redshifts is not large: the galaxy velocity dispersion  $\sigma$  and the cluster size  $R$  are sufficient to yield an estimate of the cluster total mass  $M = \sigma^2 R/G$  [82], where  $G$  is the gravitational constant. More accurate measurements require a surface term correction [70, 39], which can decrease the estimated mass by a substantial factor ( $\sim 20\%$ , on average [28]), and knowledge of the galaxy orbital distribution; however, although this distribution can only be reasonably guessed in most cases, its uncertainty has only a modest impact ( $\sim 5\%$ ) on the final mass estimate. These uncertainties become an order of magnitude larger if the galaxies are not fair tracers of the mass distribution.

When the number of galaxy spectra is large enough that we can estimate the velocity dispersion profile, we can apply the Jeans equations for a steady-state spherical system. The cumulative mass is

$$(1) \quad M(< r) = -\frac{\langle v_r^2 \rangle r}{G} \left[ \frac{d \ln \rho_m}{d \ln r} + \frac{d \ln \langle v_r^2 \rangle}{d \ln r} + 2\beta(r) \right].$$

However, as in the virial theorem, the application of equation (1) requires the assumption of a relation between the galaxy number density profile and the mass density profile  $\rho_m$ . Moreover, we do not usually know the velocity anisotropy parameter

$$(2) \quad \beta(r) = 1 - \frac{\langle v_\theta^2 \rangle + \langle v_\phi^2 \rangle}{2\langle v_r^2 \rangle},$$

where  $v_\theta$ ,  $v_\phi$ , and  $v_r$  are the longitudinal, azimuthal and radial components of the velocity  $v$  of the galaxies, respectively, and the brackets indicate an average over the velocities of

---

<sup>(1)</sup> We use  $H_0 = 100h$  km s<sup>-1</sup> Mpc<sup>-1</sup> throughout.

the galaxies in the volume  $d^3\mathbf{r}$  centered on position  $\mathbf{r}$  from the cluster center. Therefore, we can not measure  $M(< r)$  without guessing  $\beta(r)$ , or vice versa. A common strategy is to measure the velocity distributions of different galaxy populations which are assumed to be in equilibrium and thus to trace the same gravitational potential. This method can help to break this mass-anisotropy degeneracy, although not completely (see [6, 7] for very lucid reviews of these methods).

We can estimate the mass profile when observations in the X-ray band provide the intracluster medium (ICM) density  $\rho_{\text{gas}}$  and temperature  $T$ . The assumption of hydrostatic equilibrium of the ICM yields a relation similar to equation (1)

$$(3) \quad M(< r) = -\frac{kTr}{G\mu m_p} \left[ \frac{d \ln \rho_{\text{gas}}}{d \ln r} + \frac{d \ln T}{d \ln r} \right]$$

where  $k$  is the Boltzmann constant,  $\mu$  the mean molecular weight, and  $m_p$  the proton mass. Note that the term analogous to  $\beta$ , which appears in equation (2), is now zero, because, unlike the galaxy orbits, the ICM pressure is isotropic. When a sufficient angular resolution and energy sensitivity are not available to measure the X-ray spectrum at different clustrocentric radius and thus estimate the temperature profile, an isothermal ICM is usually assumed. However, the departure from this assumption appears to be substantial in most clusters where the density and temperature structures can be measured (e.g., [38, 19]).

For estimating the cluster mass when detailed observations of the cluster are unavailable, we can use a scaling relation between the mass and an observable average quantity. The most commonly used scaling relations are those involving ICM thermal properties, as the X-ray temperature (e.g. [45]; see also [9, 10] for reviews). In this case, however, the complex thermal structure of the ICM can significantly bias the cluster mass estimate [50]. Rather than using an X-ray observable, one could use, in principle, the integrated Sunyaev-Zel'dovich effect, which yields a correlation with mass which is tighter than the mass-X-ray temperature correlation [40]. However, this correlation is currently valid only for simulated clusters, and still needs to be confirmed by upcoming cluster surveys.

**2.2. Dropping the dynamical equilibrium assumption.** – The astrophysical relevance of galaxies as gravitational lenses was first intuited by Zwicky [82], but it was only fifty years later that the first gravitational lens effect was measured in a galaxy cluster [37]. The lensing effect is a distortion of the optical images of sources beyond the mass concentration; this distortion depends only on the amount of mass along the line-of-sight and not on the dynamical state of this mass. The obvious advantage is thus that the dynamical equilibrium assumption, that is essential for all the methods listed above, becomes now unnecessary. The lensing effect can be classified as strong or weak lensing, depending on its intensity. Strong lensing creates multiple images of a single source and can be used for measuring the cluster mass in its core, where the gravitational potential is deep enough. In the outer regions, the lensing effect is weaker and it only yields a tangential distortion of the induced ellipticities of the shape of the background galaxies;

weak lensing can thus measure the depth of the potential well from the center to the cluster outskirts. The most serious disadvantage of gravitational lensing for measuring masses is that the signal intensity depends on the relative distances between observer, lens and source, and not all the clusters can clearly be in the appropriate position to provide lens effects that are easily measurable. Moreover, weak lensing does not generally have a large signal-to-noise ratio and weak lensing analyses are not trivial (see e.g., [64]).

In 1997, Diaferio and Geller [22] proposed the caustic technique, a novel method to estimate the cluster mass which is not based on the dynamical equilibrium assumption and only requires galaxy celestial coordinates and redshifts. The method can thus measure the cluster mass on all the scales from the central region to well beyond the virial radius  $r_{200}$ , the radius within which the average mass density is 200 times the critical density of the Universe. Prompted by the  $N$ -body simulations of van Haarlem and van de Weygaert [76], Diaferio and Geller [22] noticed that in hierarchical models of structure formation, the velocity field in the regions surrounding the cluster is not perfectly radial, as expected in the spherical infall model [51, 30], but has a substantial random component. This fact can be exploited to extract the escape velocity of galaxies from their distribution in redshift space. Here, we will provide an overview of this method.

**2.3. Masses on different scales.** – It is clear that weak lensing and the caustic technique can be applied to scales larger than the virial radius because they do not depend on the assumption of dynamical equilibrium. However, the other estimators we mentioned above do not always measure the total cluster mass within  $r_{200}$ , as, for example, the virial analyses, based on optical observations, usually do. X-ray estimates rarely go beyond  $\sim 0.5r_{200}$ , because on these larger scales the X-ray surface brightness becomes smaller than the X-ray telescope sensitivity; gravitational lensing only measures the central mass within  $\sim 0.1r_{200}$ , where the strong regime applies. Of course, scaling relations do not provide any information on the mass profile, but they rather provide the total mass within a given radius which depends on the scaling relation used: typically, X-ray, optical and Sunyaev-Zel’dovich scaling relations yield masses within increasing radii, but still smaller than  $r_{200}$ .

### 3. – History

The spherically symmetric infall onto an initial density perturbation is the simplest classical problem we encounter when we treat the formation of cosmic structure by gravitational instability in an expanding background [29, 5]. The solution to this problem provides two relevant results: the density profile of the resulting system and the mean mass density of the Universe  $\Omega_0$ .

The former issue has a long history that we do not review here (see, e.g., [81, 20]). The basic idea is simple: we can imagine a spherical perturbation separated into individual spherical mass shells that expand to the maximum turn-around radius, the radius where the radial velocity  $v_{\text{pec}}(r)$  equals the Hubble velocity, before starting to collapse. This simple picture enables us to predict the density profile of the final object if we assume that

mass is conserved, there is no shell crossing, and we know the initial density profile of the perturbation, namely the initial two-point mass correlation function  $\xi(r)$ ;  $\xi(r)$  contains the same information as the power spectrum  $P(k)$  of the mass density perturbations, if these are Gaussian variates. For scale-free initial power spectra  $P(k) \propto k^n$ , the final density profile is  $\rho \propto r^{-\alpha}$  with  $\alpha$  depending on  $\Omega_0$  and  $n$ .

The spherically symmetric infall can also be used to estimate  $\Omega_0$ . When the average mass overdensity  $\delta(r)$  within the radius  $r$  of the perturbation is small enough, we can compute the radial velocity of each shell of radius  $r$  according to linear theory

$$(4) \quad \frac{v_{\text{pec}}(r)}{H_0 r} = -\frac{1}{3}\Omega_0^{0.6}\delta(r).$$

In the simplest application of this relation to real systems, we assume that galaxies trace mass, so that the galaxy number overdensity is simply related to  $\delta$ ; a measure of  $v_{\text{pec}}$  thus promptly yields  $\Omega_0$ . In the 1980s this strategy was applied to the Virgo cluster and the Local Supercluster; galaxies in these systems are close enough that we can measure galaxy distances  $d$  independently of redshift  $cz$ , and thus estimate the projection along the line of sight,  $v_{\text{pec}}^{\text{los}} = cz - H_0 d$ , of the radial velocity  $v_{\text{pec}}$ . These analyses indicated that  $\Omega_0 = 0.35 \pm 0.15$  [18], in agreement with the most recent estimates [25], but at odds with the inflationary value  $\Omega_0 = 1$ , which, at that time, was commonly believed to be the “correct” value.

A slight complication derives from the fact that the external regions of clusters are not properly described by linear theory. We can use instead the spherical infall model. In this case,  $\delta$  and  $\Omega_0$  are still separable quantities and we can recast equation (4) as

$$(5) \quad \frac{v_{\text{pec}}(r)}{H_0 r} = -\frac{1}{3}\Omega_0^{0.6}f(\delta)$$

so that we can still measure  $\Omega_0$  once  $\delta$  is known. Typical approximations are  $f(\delta) = \delta(1 + \delta)^{-1/4}$  [79] and  $f(\delta) = \delta(1 + \delta/3)^{-1/2}$  [77, 16]. A more serious complication is that departures from spherical symmetry can be large in real systems and the radial velocities  $v_{\text{pec}}$  derived from their line-of-sight components can be affected by relative uncertainties of the order of 50% [77].

The measure of absolute distances to galaxies remains a difficult problem today. Thus, estimating  $\Omega_0$  from the infall regions of clusters might not be trivial. However, this complication can be bypassed by the intuition of Regös and Geller [51] who were inspired by the work of Shectman [67], Kaiser [33] and Ostriker *et al.* [42]. Kaiser showed that when observed in redshift space (specifically the line-of-sight velocities of galaxies  $cz$  versus their clustrocentric angular distance  $\theta$ ), the infall pattern around a rich cluster appears as a “trumpet horn” whose amplitude  $\mathcal{A}(\theta)$  decreases with  $\theta$ . The turn-around radius is identified by the condition  $\mathcal{A}(\theta) = 0$  [42]. For the Abell cluster A539, Ostriker *et al.* [42] found the turn-around radius  $\theta_{\text{ta}} \sim 2^\circ \sim 3h^{-1}$  Mpc. Although the galaxy sampling in the infall region of this cluster was too sparse to measure  $\Omega_0$  (they only set a

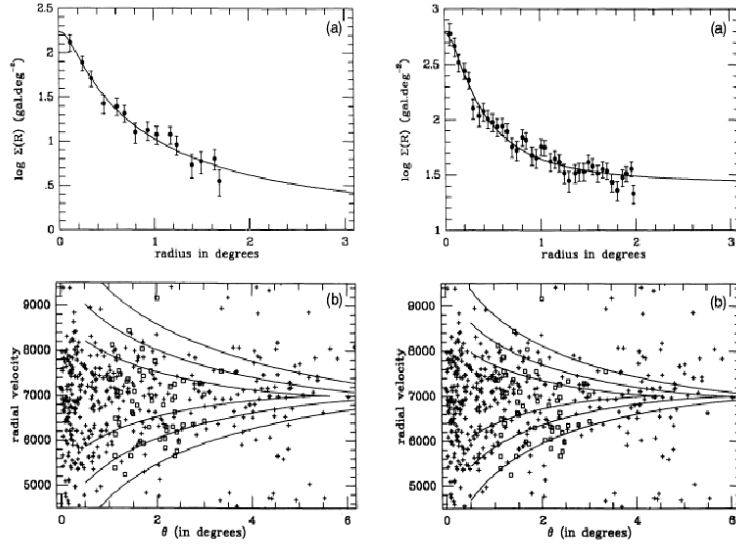


Fig. 1. – Caustics (solid lines) according to the spherical infall model (equation 7) in the Coma cluster (lower panels). The symbols show the galaxy positions in the redshift diagram. Larger amplitudes correspond to increasing cosmic densities  $\Omega_0 = 0.2, 0.5, 1.0$ . The mass overdensity  $\delta$  is estimated from the galaxy number densities (upper panels) based on CfA data (left panels), or APM data (right panels). From [75].

lower limit  $\Omega_0 > 0.03$  with equation 5), the proposed strategy was intriguing, because it was shown that measuring galaxy distances independently of redshift was unnecessary.

Regös and Geller [51] quantified this intuition by showing that the relation between the galaxy number density  $\bar{n}(r)$  in real space and the galaxy number density  $n(cz, \theta)$  in redshift space is

$$(6) \quad n(cz, \theta) = \bar{n}(r) \left( \frac{r}{cz} \right)^2 \frac{1}{J}$$

where  $J$  is the Jacobian of the transformation from real to redshift space coordinates. When  $J = 0$ ,  $n(cz, \theta)$  is infinite. This condition locates the borders of Kaiser’s horn which are named *caustics*. We can now use equation (5) to relate  $\mathcal{A}(\theta)$  to  $\Omega_0$  (equation 34 of [51]):

$$(7) \quad \mathcal{A}(\theta) \sim \Omega_0^{0.6} r f(\delta) \left[ -\frac{d \ln f(\delta)}{d \ln r} \right]^{-1/2}$$

where  $r$  and  $\theta$  are related by the transformation from real to redshift space coordinates.

Unfortunately, the caustics appeared to be very fuzzy when a sufficiently dense sampling of the infall region of a rich cluster like Coma was obtained [75]; consequently, the

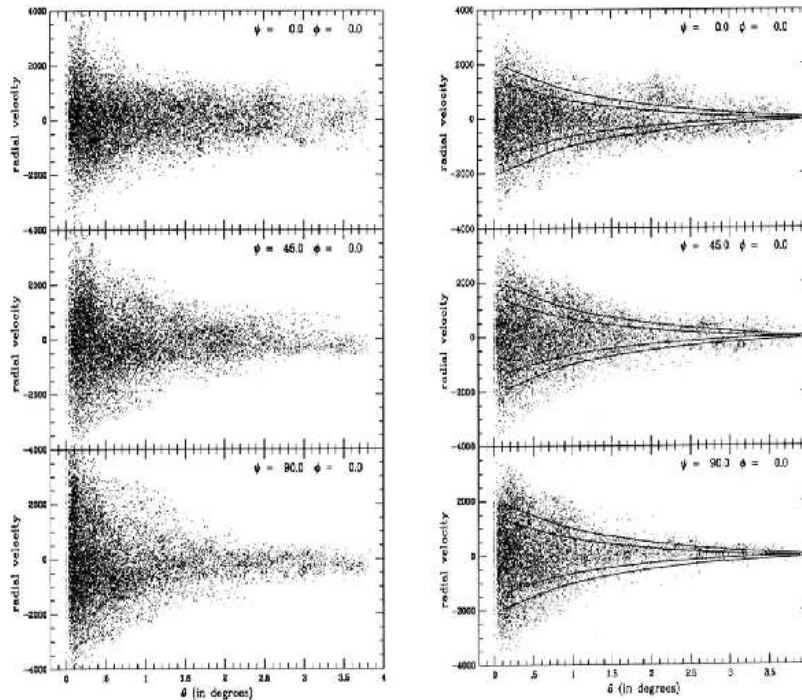


Fig. 2. – Redshift diagrams of clusters in an  $N$ -body simulation of the standard Cold Dark Matter (CDM) model with  $\Omega_0 = 1$ . The dots show the dark matter particle positions. The left column shows the redshift diagrams of the same cluster, observed along three different lines of sight, that has just accreted a group. The right column shows the redshift diagram of another cluster, observed along three different lines of sight, that has not had substantial mass accretion in the recent past. In the right column, the caustics according to the spherical infall model are also shown as solid lines; the smaller (larger) amplitude corresponds to  $\Omega_0 = 0.5$ , ( $\Omega_0 = 1$ ), whereas  $\Omega_0 = 1$  in the simulation. From [76].

measure of  $\Omega_0$  was rather uncertain (Figure 1). This disappointing result was attributed to the fact that the assumption of spherical symmetry is very poorly satisfied and that the substructure surrounding the cluster distorts the radial velocity field [76] (Figure 2). Being so sensitive to the cluster shape, locating the caustics in the redshift diagram did not appear to be a promising strategy to measure  $\Omega_0$ .

A breakthrough came when Diaferio and Geller [22] took a step further than van Haarlem and van de Weygaert. In hierarchical clustering scenarios, clusters accrete mass episodically and anisotropically [14] rather than through the gentle infall of spherical shells. Moreover, clusters accrete galaxy groups with their own internal motion. Therefore, the velocity field of the infall region can have substantial non-radial and random components. These velocity components both make the caustic location fuzzy, and, more importantly, increase the caustic amplitude when compared to the spherical infall model.

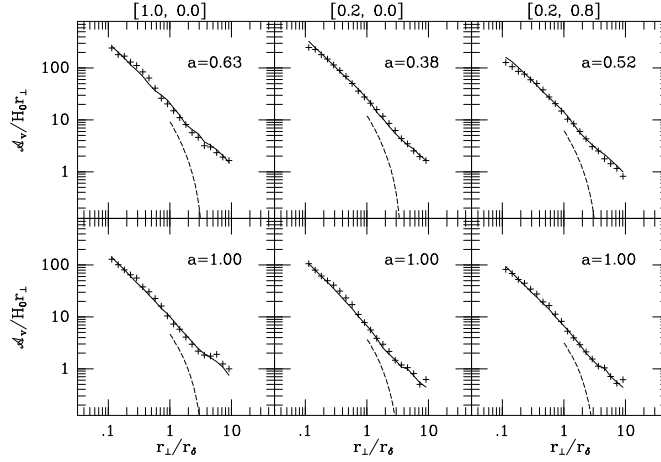


Fig. 3. – Caustic amplitude vs. projected clustrocentric distance for a simulated cluster in three different CDM cosmologies (columns) with  $[\Omega_0, \Omega_\Lambda]$  as shown above the upper panels. The cluster is shown right after a major merger (upper row) and at equilibrium (lower row). The cosmic time is shown by the scale factor  $a$ . The crosses show the actual caustic amplitude. The solid lines show the line-of-sight component of the square of the escape velocity:  $\langle v_{\text{esc,los}}^2(r) \rangle^{1/2} = \{-2\phi(r)[1 - \beta(r)]/[3 - 2\beta(r)]\}^{1/2}$ . The dashed lines show the prediction of the spherical infall model. Clustrocentric distances are in units of the virial radius  $r_\delta$ . From [22].

This intuition opened the way to interpret the square of the caustic amplitude  $\mathcal{A}^2(\theta)$  as the average, over the volume  $d^3\mathbf{r}$ , of the square of the line-of-sight component of the escape velocity  $\langle v_{\text{esc,los}}^2(r) \rangle = [-2\phi(r)g^{-1}(\beta)]^{1/2}$ , where  $\phi(r)$  is the gravitational potential profile and  $g$  (equation 10) is a function of the velocity parameter anisotropy  $\beta(r)$ . The crucial point here is that the equation  $\mathcal{A}^2(r) = \langle v_{\text{esc,los}}^2(r) \rangle$  holds *independently of the dynamical state of the cluster*.

This interpretation works amazingly well. Figure 3 shows the results of  $N$ -body simulations of the formation and evolution of a galaxy cluster in Cold Dark Matter (CDM) models with different cosmological parameters. The caustic amplitude (crosses) and  $\langle v_{\text{esc,los}}^2(r_\perp) \rangle$  (solid lines), as a function of the projected distance  $r_\perp$ , agree at all scales out to ten virial radii  $r_\delta$ <sup>(2)</sup> and independently of the dynamical state of the cluster: immediately after a major merging (upper panels) or at equilibrium (lower panels). The spherical infall model (dashed lines), which should only hold for  $r_\perp > r_\delta$ , always severely underestimates the actual caustic amplitude. These simulations and those in [21] also show another relevant result: the major effect of the cluster shape is not to make the

---

<sup>(2)</sup> See [22] for the proper definition of the virial radius  $r_\delta$  in these plots.



caustics fuzzy but rather to yield different caustic amplitudes depending on the line of sight.

The identification  $\mathcal{A}^2(r) = \langle v_{\text{esc,los}}^2(r) \rangle$  can be immediately used to measure the cluster mass. If we assume spherical symmetry, the cumulative total mass  $M(< r)$  is

$$(8) \quad GM(< r) = r^2 \frac{d\phi}{dr} = -\frac{r}{2} \langle v_{\text{esc,los}}^2 \rangle g(\beta) \left( \frac{d \ln \langle v_{\text{esc,los}}^2 \rangle}{d \ln r} + \frac{d \ln g}{d \ln r} \right).$$

However, in realistic situations, the two logarithmic derivatives are comparable, and we thus need to know  $\beta(r)$ : this is generally not the case. Moreover, the most serious obstacle in using equation (8) is the fact that sparse sampling and background and foreground galaxies yield the estimate of  $\langle v_{\text{esc,los}}^2(r) \rangle$  too noisy to extract accurate information from its differentiation.

To bypass this problem, Diaferio and Geller [22] suggested a different recipe to estimate the cumulative mass

$$(9) \quad GM(< r) = \mathcal{F}_\beta \int_0^r \langle v_{\text{esc,los}}^2(r) \rangle dr = \mathcal{F}_\beta \int_0^r \mathcal{A}^2(r) dr$$

where  $\mathcal{F}_\beta \approx 0.5$  is a constant. This recipe has been applied to a large number of clusters ever since and it is now becoming a popular tool to measure the mass in the cluster infall regions. Below, we justify this recipe and show how it works in practice.

#### 4. – The caustic method

In hierarchical clustering models of structure formation, clusters form by the aggregation of smaller systems accreting onto the cluster from the surrounding region. The accretion does not happen purely radially and galaxies within the falling clumps have velocities with substantial non-radial components. Specifically, these velocities depend both on the tidal fields of the surrounding region and on the gravitational potential of the clusters and the groups where the galaxies reside. In the previous section, we have seen that, when viewed in the redshift diagram, galaxies populate a region with a characteristic trumpet shape whose amplitude, which decreases with increasing  $r$ , is related to the escape velocity from the cluster region.

The escape velocity  $v_{\text{esc}}^2(r) = -2\phi(r)$ , where  $\phi(r)$  is the gravitational potential originated by the cluster, is a non-increasing function of  $r$ , because gravity is always attractive and  $d\phi/dr > 0$ . Thus, we can identify the square of the amplitude  $\mathcal{A}$  at the projected radius  $r_\perp$  as the average of the square of the line-of-sight component  $\langle v_{\text{los}}^2 \rangle$  of the escape velocity at the three-dimensional radius  $r = r_\perp$ . To relate  $\langle v_{\text{los}}^2 \rangle$  to  $\phi(r)$ , we need the velocity anisotropy parameter  $\beta(r)$  (equation 2). If the cluster rotation is negligible, we have  $\langle v_\theta^2 \rangle = \langle v_\phi^2 \rangle = \langle v_{\text{los}}^2 \rangle$ , and  $\langle v_r^2 \rangle = \langle v^2 \rangle - 2\langle v_{\text{los}}^2 \rangle$ . By substituting this relation into equation (2), we obtain  $\langle v^2 \rangle = \langle v_{\text{los}}^2 \rangle g(\beta)$  where

$$(10) \quad g(\beta) = \frac{3 - 2\beta(r)}{1 - \beta(r)}.$$

By applying this relation to the escape velocity at radius  $r$ ,  $\langle v_{\text{esc}}^2(r) \rangle = -2\phi(r)$ , and by assuming that  $\mathcal{A}^2(r) = \langle v_{\text{esc,los}}^2 \rangle$ , we obtain the fundamental relation between the gravitational potential  $\phi(r)$  and the observable caustic amplitude  $\mathcal{A}(r)$

$$(11) \quad -2\phi(r) = \mathcal{A}^2(r)g(\beta) .$$

To infer the cluster mass to very large radii, one first notices that the mass of a shell of infinitesimal thickness  $dr$  can be cast in the form  $Gdm = -2\phi(r)\mathcal{F}(r)dr = \mathcal{A}^2(r)g(\beta)\mathcal{F}(r)dr$  where

$$(12) \quad \mathcal{F}(r) = -2\pi G \frac{\rho(r)r^2}{\phi(r)} .$$

Therefore the mass profile is

$$(13) \quad GM(< r) = \int_0^r \mathcal{A}^2(r)\mathcal{F}_\beta(r)dr$$

where  $\mathcal{F}_\beta(r) = \mathcal{F}(r)g(\beta)$ .

Equation (13) however only relates the mass profile to the density profile of a spherical system and one profile can not be inferred without knowing the other. We can solve this impasse by noticing that, in hierarchical clustering scenarios,  $\mathcal{F}(r)$  is not a strong function of  $r$  [22]. This is easily seen in the case of the Navarro, Frenk and White (NFW) [41] mass density profile, which is an excellent description of the dark matter distribution in these models:

$$(14) \quad \mathcal{F}_{\text{NFW}}(r) = \frac{r^2}{2(r+r_s)^2} \frac{1}{\ln(1+r/r_s)}$$

where  $r_s$  is a scale-length parameter. If clusters form through hierarchical clustering,  $\mathcal{F}_\beta(r)$  is also a slowly changing function of  $r$  [22, 21]. We can then assume, somewhat strongly, that  $\mathcal{F}_\beta(r) = \mathcal{F}_\beta = \text{const}$  altogether and adopt the recipe

$$(15) \quad GM(< r) = \mathcal{F}_\beta \int_0^r \mathcal{A}^2(r)dr .$$

When  $\mathcal{F}_\beta = 1/2$ , this recipe proves to yield mass profiles accurate to 50% or better both in  $N$ -body simulations and in real clusters, when compared with masses obtained with standard methods, namely Jeans equation, X-ray and gravitational lensing, applied on scales where the validities of these methods overlap [23].

It is appropriate to emphasize that equations (11) and (13) are rigorously correct, whereas equation (15) is a heuristic recipe for the estimation of the mass profile.

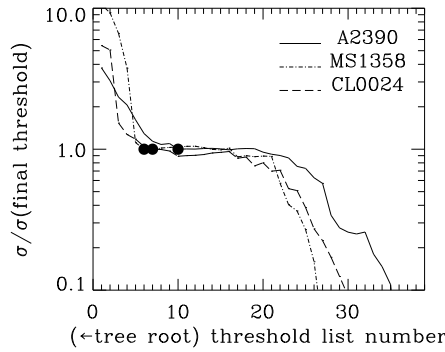


Fig. 4. – Velocity dispersion of the galaxies on the main branch of the binary tree of three real clusters while walking towards the leaves (see [23]). There is an obvious plateau when entering the tree sector with the cluster members. The filled dots indicate the chosen  $\sigma$  used to cut the binary tree and thus select the cluster members.

**4.1. Implementation.** – The implementation of the caustic method requires: (1) the determination of the cluster center; (2) the estimate of the galaxy distribution in the redshift diagram; (3) the location of the caustics.

For estimating the cluster center, the galaxies in the cluster field of view<sup>(3)</sup> are arranged in a binary tree according to the pairwise projected energy

$$(16) \quad E_{ij} = -G \frac{m_i m_j}{R_p} + \frac{1}{2} \frac{m_i m_j}{m_i + m_j} \Pi^2$$

where  $R_p$  and  $\Pi$  are the projected spatial separation and the proper line-of-sight velocity difference of each galaxy pair respectively;  $m_i$  and  $m_j$  are the galaxy masses which are usually set constant, but can also be chosen according to the galaxy luminosities.

By walking along the main branch of the tree from the root to the leaves, we progressively remove the background and foreground galaxies. We identify the cluster members by computing the velocity dispersion  $\sigma$  of the galaxies still on the main branch at each step:  $\sigma$  remains roughly constant when we move through the binary tree sector which only contains the cluster member (Figure 4), because the cluster is approximately isothermal.

The cluster members provide the cluster center and therefore the redshift diagram  $(r, v)$ . The galaxy distribution  $f_q(r, v)$  on this plane is estimated with an adaptive kernel method. At each projected radius  $r$ , the function  $\varphi(r) = \int f_q(r, v) dv$  provides the mean escape velocity  $\langle v_{\text{esc}}^2 \rangle_{\kappa, R} = \int_0^R \mathcal{A}_\kappa^2(r) \varphi(r) dr / \int_0^R \varphi(r) dr$  where  $\mathcal{A}_\kappa$  is the amplitude of the caustics located by the equation  $f_q(r, v) = \kappa$ . The appropriate  $\kappa$  is the root of the

---

<sup>(3)</sup> We clarify that to apply the caustic technique we already need to know that there is a cluster in the field of view. The caustic technique, as it is currently conceived, is not a method to identify clusters in redshift surveys, as the Voronoi tessellation [48] or the matched filter [47].

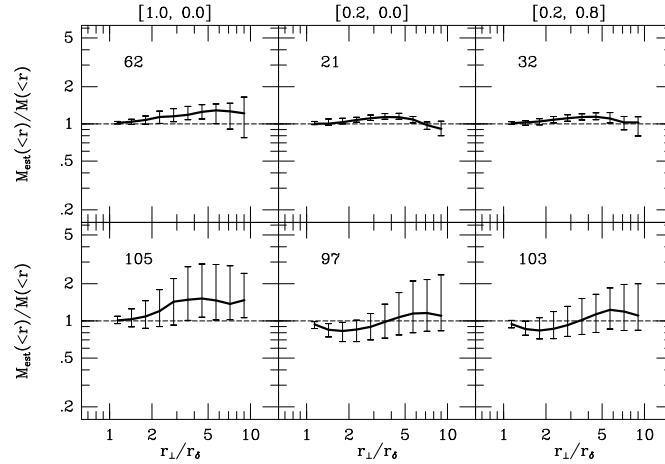


Fig. 5. – Median mass profiles, measured with the caustic technique, of dark matter halos in samples extracted from CDM models. The cosmological parameters  $[\Omega_0, \Omega_\Lambda]$  are shown above the upper panels. The upper row shows the most massive halos:  $M(< r_\delta) \geq 10^{14} M_\odot$  for the high-density model, and  $M(< r_\delta) \geq 2 \cdot 10^{13} M_\odot$  for the low-density models. The lower row shows the least massive halos:  $10^{13} M_\odot \leq M(< r_\delta) < 10^{14} M_\odot$  for the high-density model, and  $10^{12} M_\odot \leq M(< r_\delta) < 2 \cdot 10^{13} M_\odot$  for the low-density models. The numbers of halos in each sample are indicated in each panel. The error bars indicate upper and lower quartiles at each projected distance  $r_\perp$ . From [22].

equation  $\langle v_{\text{esc}}^2 \rangle_{\kappa, R} = 4\sigma^2$ , where  $\sigma^2$  is the velocity dispersion of the members identified on the binary tree. Further technical details of this implementation are described in [21, 66].

## 5. – Reliability of the method

**5.1. Comparison with simulations.** – The caustic technique was tested on  $N$ -body simulations of cluster formation in CDM cosmologies. Dark matter only simulations showed that the caustic amplitude and the escape velocity profiles agree amazingly well out to ten virial radii, independently of the cosmological parameters and, more importantly, of the dynamical state of the cluster (Figure 3). These simulations also showed that the technique works on both massive and less massive clusters (Figure 5). In the latter case, the scatter is larger because of projection effects and sparse sampling. In the most massive systems, the mass is recovered within 20% out to ten virial radii in most cases.

To test the implementation of the caustic method in realistic cases, we can use  $N$ -body simulations where the galaxies are formed and evolved with a semi-analytic technique [34]. Figure 6 shows the mass profile of a single cluster observed along ten different lines of sight in such simulations [21]. When comparing this figure with Figures 3 and 5, where all the dark matter particles were observed, we see that the caustic technique performs in

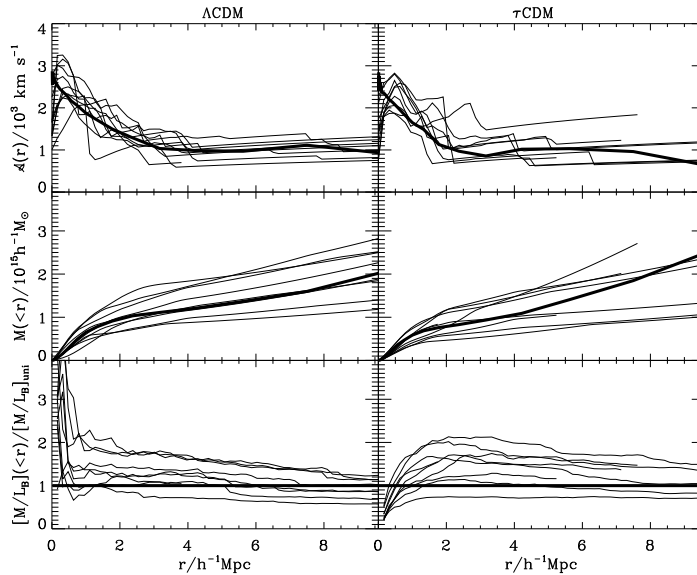


Fig. 6. – Radial profiles of the caustic amplitude (upper row), cumulative mass (middle row), and mass-to-light ratio (lower row) of a simulated cluster observed along ten different lines of sight. The thin lines are the profiles estimated from the individual redshift diagrams. The thick lines are the real profiles. In the lower panels, the solid line is the mean mass-to-light ratio of the simulated universe. Left and right columns are for a cluster in a  $\Lambda$ CDM and a  $\tau$ CDM model, respectively. From [21].

this latter case better than when only the galaxies are available. This difference clearly originates from the sparser sampling of the velocity field provided by the galaxies. Figure 6 also shows that projection effects cause the most relevant systematic error. However, the uncertainty on the mass profile remains smaller than 50% out to  $8h^{-1}$  Mpc from the cluster center.

**5.2. Caustic vs. lensing.** – In equation (15) the choice of the constant filling factor  $\mathcal{F}_{\beta}$  is based on  $N$ -body simulations alone. Therefore, it is not guaranteed that the caustic technique can recover the mass profile of real clusters if the simulations are not a realistic representation of the large-scale mass distribution in the Universe.

Other than the caustic technique, the only method for estimating the mass in the outer regions of galaxy clusters is based on weak lensing. The comparison between these two methods was performed on the clusters A2390, MS1358 and Cl 0024 which are at the appropriate redshift to have a reasonably intense lens signal and a sufficiently high number of galaxy redshifts [23]. Figure 7 shows the redshift diagrams and the mass profiles of these systems. Caustic and lensing masses agree amazingly well. The most impressive result is for Cl 0024. This cluster is likely to have experienced a recent merging event [17], and it probably is out of equilibrium: in this system the caustic mass and the

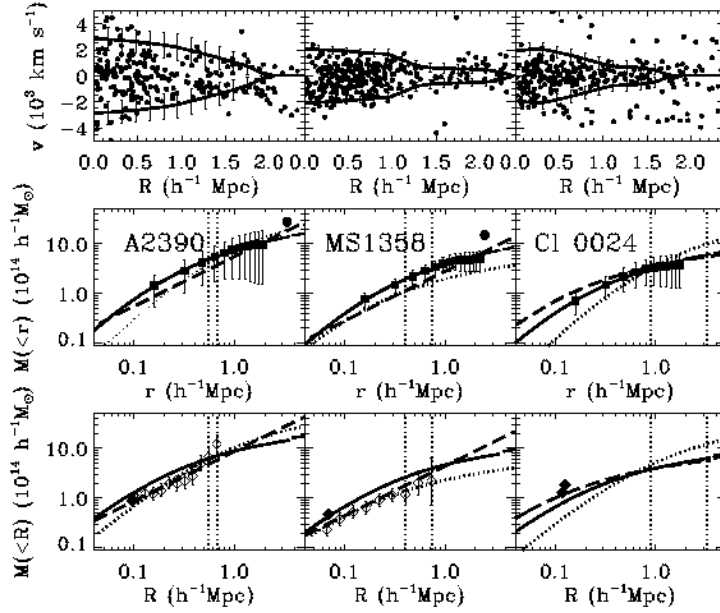


Fig. 7. – Comparison between caustic, lensing, and X-ray mass estimates. The left, middle and right columns are for A2390, MS1358 and Cl 0024, respectively. *Top panels:* Redshift diagrams with the galaxies (dots) and caustic locations (solid lines). Line-of-sight velocities  $v$  are in the cluster rest-frame. *Middle panels:* Three-dimensional cumulative mass profiles. The solid squares show the caustic mass estimates; the solid lines are the best-fitting NFW profiles to the data points within  $1h^{-1}$  Mpc; the dotted lines are the best-fitting NFW profiles to the X-ray measures (from left to right: [2, 3, 43]); the dashed lines are the best-fitting isothermal (A2390, [69]; MS1358, [31]) or NFW models (Cl 0024, [35]) to the gravitational lensing measures. The left and right vertical dotted lines show the radius of the X-ray and gravitational lensing fields of view, respectively. The two filled circles show the virial estimates of A2390 and MS1358 [12]. *Bottom panels:* Projected cumulative mass profiles; lines are as in the middle panels. The open diamonds show the weak lensing measures: A2390, [69]; MS1358, lower limit to the mass profile [31]. Filled diamonds show the strong lensing measures: A2390, [46]; MS1358: [1, 26]; Cl 0024: upper symbol, [73], lower symbol, [11]. Error bars in all panels are  $1\text{-}\sigma$ ; error bars on points where they seem to be missing are smaller than the symbol size. From [23].

lensing mass agree with each other, but disagree with the X-ray mass, which is the only estimate relying on dynamical equilibrium. This result therefore proves the reliability of the caustic technique and its independence of the dynamical state of the system in real clusters.

## 6. – Application to real systems

**6.1. Mass profiles.** – Geller *et al.* [27] were the first to apply the caustic method to a real cluster: they measured the mass profile of Coma out to  $10h^{-1}$  Mpc from the cluster

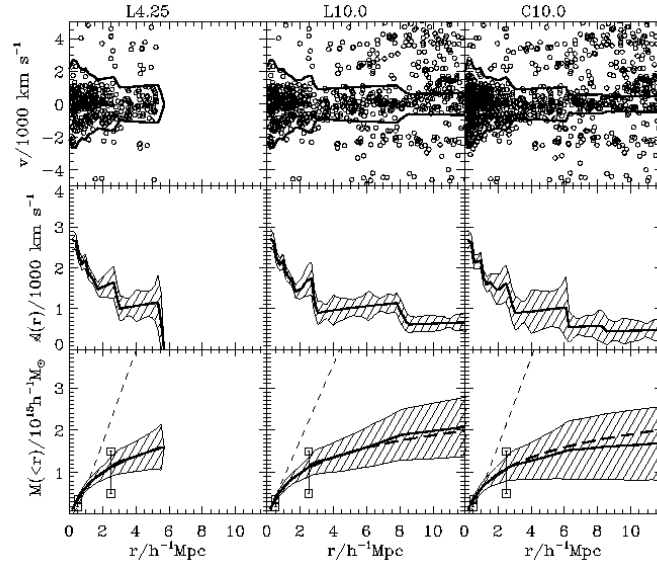


Fig. 8. – **Top panels:** Galaxy distribution in the redshift diagram of Coma for three galaxy samples of increasing size. There are 332, 480, and 691 galaxies within the caustics in the samples L4.25, L10.0, and C10.0, respectively. Note that these samples are not substantially larger than the samples in Figure 1 used to estimate  $\Omega_0$  with the spherical infall model. The bold lines indicate the location of the caustics. Half the distance between the caustics defines the amplitude  $A(r)$  shown in the middle panels. **Bottom panels:** The bold lines are the caustic mass profiles. The two error bars show the range of the X-ray mass estimates listed in [32]. Short-dashed and long-dashed lines are the cumulative mass profile for a softened isothermal sphere and an NFW density profile with parameters obtained by fitting the mass profile in the range  $[0, 1]h^{-1}$  Mpc. Shaded areas in the middle and bottom panels indicate the  $2\text{-}\sigma$  uncertainty. From [23].

center and were able to demonstrate that the NFW profile fits the cluster density profile out to these very large radii, thus ruling out the isothermal sphere as a viable model of the cluster mass distribution (Figure 8). A few years later, the failure of the isothermal model was confirmed by the first similar analyses based on gravitational lensing applied to A1689 [13, 36] and Cl 0024 [35]. The goodness of the NFW fit out to  $5 - 10h^{-1}$  Mpc was confirmed by applying the caustic technique to a sample of nine clusters densely sampled in their outer regions, the Cluster And Infall Region Nearby Survey (CAIRNS, [61]), and, more recently, to a complete sample of 72 X-ray selected clusters with galaxy redshifts extracted from the Fourth Data Release of the Sloan Digital Sky Survey (Cluster Infall Regions in the Sloan Digital Sky Survey: CIRS, [54]).

CIRS is currently the largest sample of clusters whose mass profiles have been measured out to  $\sim 3r_{200}$  (Figure 9); Rines and Diaferio [54] were thus able to obtain a statistically significant estimate of the ratio between the mass within the turn-around radius  $M_t$  and the virial mass  $M_{200}$ : they found an average value of  $M_t/M_{200} = 2.2 \pm 0.2$ ,

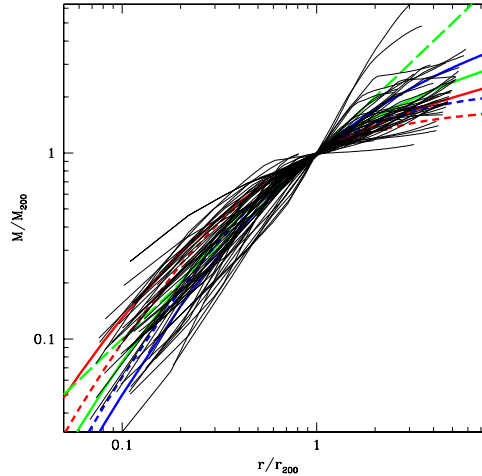


Fig. 9. – Scaled caustic mass profiles for the CIRS clusters. The thin solid lines show the caustic mass profiles normalized by  $r_{200}$  and  $M_{200}$ , the total mass within  $r_{200}$ . The long-dashed line shows a singular isothermal sphere, the solid lines show NFW profiles (with concentrations  $c = 3, 5, 10$  from top to bottom at large radii). The short-dashed lines are Hernquist profiles with scale radii different by a factor of two. From [54].

which is  $\sim 50\%$  smaller than the value expected in current models of cluster formation [71]. The caustic technique is not limited to clusters, but, when enough redshifts are available, it can also be applied to groups of galaxies: on a sample of 16 groups both the NFW mass profiles and the ratio  $M_t/M_{200} = 2.3 \pm 0.4$  are confirmed [53].

Rines *et al.* [56, 55] also used the CIRS sample to estimate the virial mass function of nearby clusters and determined cosmological parameters consistent with the WMAP values [25]; they also showed that velocity bias is absent in real clusters.

A good fit with the NFW profile out to  $\sim 2r_{200}$  was also found by Biviano and Girardi [8] who applied the caustic technique to an ensemble cluster obtained by stacking 43 clusters from the Two Degree Galaxy Redshift Survey (2dGFRS, [15]): here, unlike the previous analyses, the caustic method was not applied to individual clusters, because the number of galaxies per cluster was relatively small.

The caustic method does not rely on the dynamical state of the cluster and its external regions: there are therefore estimates of the mass of unrelaxed systems, for example, among others, the Shapley supercluster [52], the poor Fornax cluster, which contains two distinct dynamical components [24], the A2199 complex [58].

**6.2. Mass-to-light profiles.** – By combining accurate photometry with the caustic mass of A576, Rines *et al.* [59] were able to measure, for the first time, the profile of the mass-to-light ratio  $M/L$  well beyond the cluster virial radius: they found an  $R$ -band  $M/L$  profile steadily decreasing from  $\sim 0.5$  to  $4h^{-1}$  Mpc, indicating that, in this cluster, dark



matter is more concentrated than galaxies. Slightly decreasing  $M/L$  profiles were also measured in the outer region of five (including A576) out of the nine CAIRNS clusters in the  $K$ -band [57]. The remaining CAIRNS clusters have an  $M/L$  profile which remains roughly flat at radii larger than  $\sim 1h^{-1}$  Mpc. Coma shows a remarkably flat  $K$ -band  $M/L$  profile out to  $10h^{-1}$  Mpc [62]. A flat  $M/L$  profile beyond  $\sim 0.5h^{-1}$  Mpc was also found in A1644 in the  $H$ -band [72].

These results are due to two reasons: (1) a larger predominance of less luminous late-type galaxies in the cluster outer regions; and (2) the fact that the  $K$ -band  $M/L$  ratio of real galaxy systems increases with the system mass [49]. In fact, clusters form by accretion of smaller systems, as indicated for example by the optical and X-ray observations of the A2199 complex [63], and as expected in current hierarchical models of structure formation [68]; therefore, the cluster surrounding regions, which mostly contain galaxy groups, should naturally have smaller  $M/L$ . The positive  $M/L$ –mass correlation was also obtained in semi-analytical models of galaxy formation [34] and is well described by the statistical technique based on the conditional luminosity function [74].

The infall regions are the transition between the dense cluster regions and the field [4, 44], and the internal properties of galaxies do not vary abruptly at the virial radius [60]. Therefore galaxy surveys in the outskirts of clusters, as those mentioned above, can clearly constrain models of cluster and galaxy formation.

## 7. – Conclusion and perspectives

The caustic method and gravitational lensing are the only two techniques currently available for measuring the mass profile of clusters beyond their virial radius. The caustic method requires a sufficiently dense redshift survey with a large field of view and is only limited by the time needed to measure a large enough number of galaxy spectra; this observing time increases quickly with cluster redshift. On the other hand, lensing requires wide-field photometric surveys that need high angular resolution and extremely good observing conditions; moreover, the lensing signal is strong enough only when the cluster is within a limited redshift range  $z \approx 0.1 - 1$ .

When the caustic technique was proposed, multi-object spectroscopy was not routinely applied to measure galaxy redshifts, and the request of 100 or more redshifts in the outskirts of clusters appeared demanding. Nowadays this task can be accomplished more easily and the popularity of the caustic technique has begun to increase.

The caustic technique has been tested on  $N$ -body simulations and the mass profiles are accurate to better than  $\sim 50\%$  out to  $\sim 3 - 4r_{200}$ . On the three systems where both the caustic method and lensing could be applied, the two methods yield consistent mass profiles. This consistency also holds in Cl 0024 whose X-ray mass profile disagrees with the caustic and lensing profiles; this disagreement is most likely due to the fact that this cluster is out of equilibrium and thus the X-ray mass is unreliable.

The uncertainties on the caustic mass profile are almost totally due to projection effects. In fact, the method assumes that the cluster is spherically symmetric, and this is rarely the case; therefore the redshift diagram from which the caustic mass is extracted

can vary substantially when the cluster is observed along different lines of sight. The size of this systematic error is comparable to the systematic uncertainty we have with lensing methods which measure all the mass projected along the line of sight.

What the caustic technique actually measures is the line-of-sight component of the escape velocity from the cluster (equation 11). If we can measure the velocity anisotropy parameter  $\beta$ , the caustic technique thus yields a direct measure of the profile of the cluster gravitational potential.

This brief review shows that the caustic technique is a powerful tool for the analysis of clusters and their external regions, but its full potentiality still needs to be exploited. For example, the  $\sigma$  plateau, that appears when walking along the binary tree (Figure 4), provides a clean way to identify the cluster members. This issue still needs a throughout investigation [66], but very preliminary results, based on a large sample of synthetic clusters, show that  $\sim 90\%$  of the galaxies within the caustics are cluster members and that the interloper contamination is comparable or lower than other methods [78]. An additional byproduct of the caustic machinery is the identification of cluster substructures from the distribution of the galaxies in the binary tree [65]. This topic has also been currently investigated [66].

\* \* \*

I thank Alfonso Cavaliere and Yoel Rephaeli for the invitation to this fruitful and well organized school. It is a pleasure to acknowledge the hospitality of SIF during my stay in Varenna. I wish to thank Margaret Geller and Ken Rines who largely contributed to the development and dissemination of the caustic method. I also thank them for a careful reading of the manuscript and suggestions. Support from the PRIN2006 grant ‘‘Costituenti fondamentali dell’Universo’’ of the Italian Ministry of University and Scientific Research and from the INFN grant PD51 is gratefully acknowledged.

## REFERENCES

- [1] ALLEN S. W., *MNRAS*, **296** (1998) 392.
- [2] ALLEN S. W., ETTORI S. and FABIAN A. C., *MNRAS*, **324** (2001) 877.
- [3] ARABADJIS J. S., BAUTZ M. W. and GARMIRE G. P., *Astroph. J.*, **572** (2002) 66.
- [4] BALOGH M., ET AL., *MNRAS*, **348** (2004) 1355.
- [5] BERTSCHINGER E., *Astroph. J. Suppl.*, **58** (1985) 39.
- [6] BIVIANO A., in *From dark halos to light*, Proceedings of the XLI Rencontres de Moriond, XXVI Astrophysics Moriond Meeting, edited by Tresse L., Maurogordato S. and Tran Thanh Van J. (Editions Frontieres) 2006, arXiv:astro-ph/0607040.
- [7] BIVIANO A., this volume.
- [8] BIVIANO A. and GIRARDI M., *Astroph. J.*, **585** (2003) 205.
- [9] BORGANI S., astro-ph/0605575.
- [10] BORGANI S., DIAFERIO A., DOLAG K. and SCHINDLER S., *SSR*, **134** (2008) 269.
- [11] BROADHURST T., HUANG X., FRYE B., and ELLIS R., *Astroph. J. Lett.*, **534** (2000) L15.
- [12] CARLBERG R. G., YEE H. K. C., ELLINGSON E., ABRAHAM R., GRAVEL P., MORRIS S. and PRITCHET C. J. , *Astroph. J.*, **462** (1996) 32.
- [13] CLOWE D. and SCHNEIDER P., *Astron. & Astroph.*, **379** (2001) 384.

- [14] COLBERG J. M., WHITE S. D. M., JENKINS A. and PEARCE F. R., *MNRAS*, **308** (1999) 593.
- [15] COLLESS M., ET AL., *MNRAS*, **328** (2001) 1039.
- [16] CUPANI G., MEZZETTI M., and MARDIROSSIAN F., *MNRAS*, **390** (2008) 645.
- [17] CZOSKE O., MOORE B., KNEIB J.-P. and SOUCAIL G., *Astron. & Astroph.*, **386** (2002) 31.
- [18] DAVIS M. and PEEBLES P. J. E., *Ann. Rev. Astron. Astrophys.*, **21** (1983) 109.
- [19] DE GRANDI S. and MOLENDI S., *Astroph. J.*, **567** (2002) 163.
- [20] DEL POPOLO A. and GAMBERA M., astro-ph/0401609.
- [21] DIAFERIO A., *MNRAS*, **309** (1999) 610.
- [22] DIAFERIO A. and GELLER M. J., *Astroph. J.*, **481** (1997) 633.
- [23] DIAFERIO A., GELLER M. J. and RINES K., *Astroph. J. Lett.*, **628** (2005) L97.
- [24] DRINKWATER M. J., GREGG M. D. and COLLESS M., *Astroph. J. Lett.*, **548** (2001) L139.
- [25] DUNKLEY J., ET AL., arXiv:0803.0586.
- [26] FRANX M., ILLINGWORTH G. D., KELSON D. D., VAN DOKKUM P. G., and TRAN K.-V., *Astroph. J.*, **486** (1997) L75.
- [27] GELLER M. J., DIAFERIO A. and KURTZ M. J., *Astroph. J. Lett.*, **517** (1999) L23.
- [28] GIRARDI M., GIURICIN G., MARDIROSSIAN F., MEZZETTI M. and BOSCHIN W., *Astroph. J.*, **505** (1998) 74.
- [29] GUNN J. E. and GOTT J. R. III, *Astroph. J.*, **176** (1972) 1.
- [30] HIOTELIS N., *Astron. & Astroph.*, **375** (2001) 338.
- [31] HOEKSTRA H., FRANX M., KUIJKEN K. and SQUIRES G., *Astroph. J.*, **504** (1998) 636.
- [32] HUGHES J. P., *Astroph. J.*, **337** (1989) 21.
- [33] KAISER N., *MNRAS*, **227** (1987) 1.
- [34] KAUFFMANN G., COLBERG J. M., DIAFERIO A. and WHITE S. D. M., *MNRAS*, **303** (1999) 188.
- [35] KNEIB J.-P., ET AL., *Astroph. J.*, **598** (2003) 804.
- [36] LEMZE D., BROADHURST T., REPHAELI Y., BARKANA R. and UMETSU K., arXiv:0810.3129.
- [37] LYNDS R. and PETROSIAN V., *BAAS*, **18** (1986) 1014.
- [38] MARKEVITCH M., FORMAN W. R., SARAZIN C. L. and VIKHLININ A., *Astroph. J.*, **503** (1998) 77.
- [39] MERRITT D., *Astroph. J.*, **313** (1987) 121.
- [40] MOTL P. M., HALLMAN E. J., BURNS J. O. and NORMAN M. L., *Astroph. J. Lett.*, **623** (2005) L63.
- [41] NAVARRO J. F., FRENK C. S. and WHITE S. D. M., *Astroph. J.*, **490** (1997) 493.
- [42] OSTRIKER E. C., HUCHRA J. P., GELLER M. J. and KURTZ M. J., *Astron. J.*, **96** (1988) 1775.
- [43] OTA N., POINTECOUTEAU E., HATTORI M. and MITSUDA K., *Astroph. J.*, **601** (2004) 120.
- [44] *Outskirts of Galaxy Clusters: Intense Life in the Suburbs*, Proceedings of the IAU Coll. 195, edited by DIAFERIO A. (Cambridge University Press, Cambridge) 2004.
- [45] PIERPAOLI E., BORGANI S., SCOTT D. and WHITE M., *MNRAS*, **342** (2003) 163.
- [46] PIERRE M., LE BORGNE J. F., SOUCAIL G., and KNEIB J. P., *Astron. & Astroph.*, **311** (1996) 413.
- [47] POSTMAN M., LUBIN L. M., GUNN J. E., OKE J. B., HOESSEL J. G., SCHNEIDER D. P. and CHRISTENSEN J. A., *Astron. J.*, **111** (1996) 615.
- [48] RAMELLA M., BOSCHIN W., FADDA D., and NONINO M., *Astron. & Astroph.*, **368** (2001) 776.
- [49] RAMELLA M., BOSCHIN W., GELLER M. J., MAHDAVI A. and RINES K., *Astron. J.*, **128** (2004) 2022.

- [50] RASIA E., ET AL., *MNRAS*, **369** (2006) 2013.
- [51] REGÖS E. and GELLER M. J., *Astron. J.*, **98** (1989) 755.
- [52] REISENEGGER A., QUINTANA H., CARRASCO E. R. and MAZE J., *Astron. J.*, **120** (2000) 523.
- [53] RINES K. and DIAFERIO A., arXiv:0809.4015.
- [54] RINES K. and DIAFERIO A., *Astron. J.*, **132** (2006) 1275.
- [55] RINES K., DIAFERIO A. and NATARAJAN P., *Astroph. J. Lett.*, **679** (2008) L1.
- [56] RINES K., DIAFERIO A. and NATARAJAN P., *Astroph. J.*, **657** (2007) 183.
- [57] RINES K., GELLER M. J., DIAFERIO A., KURTZ M. J. and JARRETT T. H., *Astron. J.*, **128** (2004) 1078.
- [58] RINES K., GELLER M. J., DIAFERIO A., MAHDAVI A., MOHR J. J., and WEGNER G., *Astron. J.*, **124** (2002) 1266.
- [59] RINES K., GELLER M. J., DIAFERIO A., MOHR J. J., and WEGNER G. A., *Astron. J.*, **120** (2000) 2338.
- [60] RINES K., GELLER M. J., KURTZ M. J., and DIAFERIO A., *Astron. J.*, **130** (2005) 1482.
- [61] RINES K., GELLER M. J., KURTZ M. J., and DIAFERIO A., *Astron. J.*, **126** (2003) 2152.
- [62] RINES K., GELLER M. J., KURTZ M. J., DIAFERIO A., JARRETT T. H., and HUCHRA J. P., *Astroph. J. Lett.*, **561** (2001) L41.
- [63] RINES K., MAHDAVI A., GELLER M. J., DIAFERIO A., MOHR J. J., and WEGNER G., *Astroph. J.*, **555** (2001) 558.
- [64] SCHNEIDER P., in *Gravitational lensing: strong, weak and micro* edited by MEYLAN G., JETZER P. and NORTH P. (Saas-Fee Advanced Course 33, Berlin: Springer) 2006, p. 1.
- [65] SERNA A. and GERBAL D., *Astron. & Astroph.*, **309** (1996) 65.
- [66] SERRA A. L. ET AL., *in preparation*.
- [67] SHECTMAN S. A., *Astroph. J.*, **262** (1982) 9.
- [68] SPRINGEL V., FRENK C. S. and WHITE S. D. M., *Nature*, **440** (2006) 1137.
- [69] SQUIRES G., KAISER N., FAHLMAN G., BABUL A. and WOODS D., *Astroph. J.*, **469** (1996) 73.
- [70] THE L. S. and WHITE S. D. M., *Astron. J.*, **92** (1986) 1248.
- [71] TINKER J. L., WEINBERG D. H., ZHENG Z. and ZEHAZI I., *Astroph. J.*, **631** (2005) 41.
- [72] TUSTIN A. W., GELLER M. J., KENYON S. J. and DIAFERIO A., *Astron. J.*, **122** (2001) 1289.
- [73] TYSON J. A., KOCHANSKI G. P. and DELL'ANTONIO I. P., *Astroph. J. Lett.*, **498** (2001) L107.
- [74] VAN DEN BOSCH F., YANG X. and MO H. J., in *Baryons in Dark Matter Halos* edited by DETTMAR R., KLEIN U. and SALUCCI P. (SISSA, Proceedings of Science) 2004, p. 41.1.
- [75] VAN HAARLEM M. P., CAYON L., GUTIERREZ DE LA CRUZ C., MARTINEZ-GONZALEZ E. and REBOLO R., *MNRAS*, **264** (1993) 71.
- [76] VAN HAARLEM M. P. and VAN DE WEYGAERT R., *Astroph. J.*, **418** (1993) 544.
- [77] VILLUMSEN J. V. and DAVIS M., *Astroph. J.*, **308** (1986) 499.
- [78] WOJTAK R., LOKAS E. L., MAMON G. A., GOTTLÖBER S., PRADA F. and MOLES M., *Astron. & Astroph.*, **466** (2007) 437.
- [79] YAHIL A., in *The Virgo Cluster* edited by RICHTER O. and BINGGELI B. (ESO, Garching) 1985, p. 359-373.
- [80] ZAROUBI S., BRANCHINI E., HOFFMAN Y. and DA COSTA L., *MNRAS*, **336** (2002) 1234.
- [81] ZAROUBI S., NAIM A. and HOFFMAN Y., *Astroph. J.*, **457** (1996) 50.
- [82] ZWICKY F., *Astroph. J.*, **86** (1937) 217.